

Negative Differential Resistance in Carbon Atomic Wire-Carbon Nanotube Junctions

Khoong Hong Khoo,^{†‡} J. B. Neaton,^{*§} Young Woo Son,^{||,⊥} Marvin L. Cohen,^{†‡} and Steven G. Louie^{†‡§}

Department of Physics, University of California at Berkeley, Berkeley, California 94720, Materials Sciences Division, and The Molecular Foundry, Lawrence Berkeley National Laboratory, Berkeley, California 94720, Department of Physics, Konkuk University, Seoul 143-701, Korea and School of Computational Science, Korea Institute for Advanced Study, Seoul 130-722, Korea

Received June 15, 2008; Revised Manuscript Received July 21, 2008

ABSTRACT

Negative differential resistance (NDR) was recently observed in carbon nanotube junctions just before breaking and hypothesized to arise from the formation of monatomic carbon wires in the junction. Motivated by these results, a first-principles scattering-state approach, based on density functional theory, is used to study the transport properties of carbon chains covalently connecting metallic carbon nanotube leads at finite bias. The $I-V$ characteristics of short carbon chains are predicted to exhibit even-odd behavior, and NDR is found for both even and odd chain junctions in our calculations.

In recent years, there has been significant interest in the study of electron transport through individual molecules and atomic wires, motivated by the prospect of using molecules as components in atomic-scale circuits. Understanding electron transport in the ultimate limit of devices consisting of just a single molecule or a few atoms is challenging, but recent experiments have made significant progress. Several past experimental studies have reported transport properties of atomic wires and point-contacts made from monovalent metals Au,¹⁻⁷ Ag,^{5,7} Cu,^{5,8} and Na,⁸ and transition metals Pt,^{3,4,9} Pd,⁹ Ir,³ Co,⁹ and Ni⁴. Novel phenomena have been observed, such as conductance quantization¹⁻⁸ and length dependent conductance oscillations.³ These findings have often been corroborated by theoretical studies,¹⁰⁻¹⁸ employing techniques that combine density functional theory with either the nonequilibrium Green's function (NEGF)¹⁹⁻²² or scattering-state formalisms.²³⁻²⁵ These methods, in principle, allow the study of steady-state electron transport of nonequilibrium systems at finite bias voltages and have made possible the exploration of nonlinear transport phenomena such as negative differential resistance (NDR) in C and Na atomic chains.^{12,14,16} However, experimental

confirmation of these predictions is difficult, primarily because of complications in fabricating stable atomic chains capable of sustaining the high bias voltages required to achieve NDR.

Recently, the $I-V$ characteristics of short chains of carbon atoms have been reported in connection with carbon nanotube "thinning" measurements, in situ experiments in which the diameter of an individual carbon nanotube is controllably decreased by a combination of defect formation via electron irradiation, electromigration, and annealing via resistive heating.²⁶ By constructing nanotube circuits on an electronically transparent membrane, simultaneous transmission electron microscope (TEM) imaging and electrical characterization of carbon nanotubes allowed the diameter dependence of nanotube $I-V$ characteristics to be studied. Interestingly, NDR was observed for nanotubes with diameters approaching zero, the limit of a carbon atomic wire. Drawing on earlier theoretical predictions,^{12,14} it was hypothesized that the experimentally measured NDR in the $I-V$ characteristic originates with an atomic carbon chain being formed and electrically bridging a nanotube junction.

Although linearly bonded carbon atomic chains under ambient conditions are expected to be unstable, several previous works have observed carbon chain formation. Molecular dynamics simulations predicted the formation of monatomic carbon chains during the last stages of strain induced carbon nanotube fracture,^{27,28} as well as the unravel-

* To whom correspondence should be addressed. E-mail: jbneaton@lbl.gov.

† University of California at Berkeley.

‡ Materials Sciences Division, Lawrence Berkeley National Laboratory.

§ The Molecular Foundry, Lawrence Berkeley National Laboratory.

|| Konkuk University.

⊥ Korea Institute for Advanced Study.

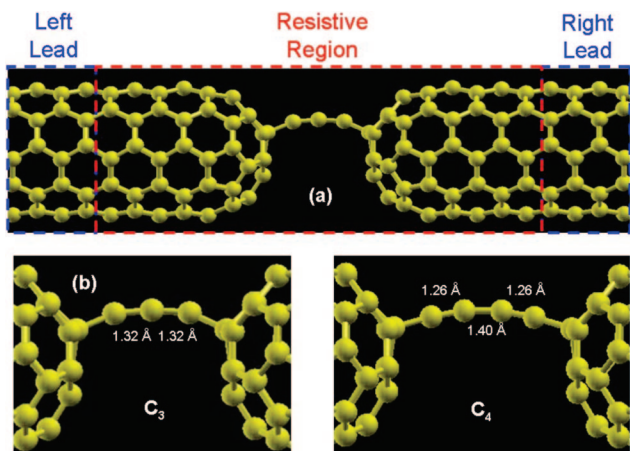


Figure 1. (a) Model geometry for scattering-state calculations consisting of a C_3 chain bridging (5,5) carbon nanotubes. (b) Bond lengths of C_3 and C_4 chains sandwiched between nanotube contacts.

ing of open-ended carbon nanotube tips to form linear chains of carbon atoms during field emission.²⁹ The NDR predicted by previous first-principles transport studies has been shown to be as much a property of the contacts as the carbon wires themselves,¹⁴ and thus further calculations of the I – V characteristics with carbon nanotube leads are clearly needed. In this work, we test the experimental hypothesis that a carbon wire covalently bridges the gap between nanotube electrodes using a first-principles scattering-state method. We calculate the I – V characteristics and investigate the physical principles underlying the transport behavior of carbon chains bridging carbon nanotubes. We find that the carbon chains exhibit clear even–odd behavior, and that both even and odd chains exhibit NDR in their I – V characteristics, consistent with the empirical hypothesis.

To calculate transport properties of nanostructures, we employ a first-principles scattering-state approach²⁵ as implemented in the SCARLET code which is based on density functional theory (DFT) and the localized basis methodology of the SIESTA package.³⁰ All calculations are performed within the local density approximation (LDA),³¹ and with norm-conserving pseudopotentials.³² We employ a single- ζ pseudoatomic orbital basis set, which has been shown to be acceptable for nanotube-based systems.^{33,34} Increasing the basis set did not result in qualitative differences and did result in only minor quantitative differences.

Our junction consists of a carbon chain connected to two semi-infinite leads, equilibrated at different chemical potentials. The junction is divided into three subsystems: the left lead, the right lead, and a finite central resistive region, consisting of the linear chain sandwiched between several buffer lead layers. The number of lead layers is chosen so that those at the interface to the left and right leads are bulk-like. The Hamiltonian matrices for the semi-infinite left and right leads are obtained from standard first-principles calculations on bulk periodic systems. For calculations at finite bias, the two leads are fixed at different chemical potentials, and a solution of the Laplace equation is added to the periodic solution of the Poisson equation of the resistive region.²⁵

Once the Hamiltonian is obtained, energy-dependent scattering states are constructed on a fine energy grid around the Fermi energy, with incoming and outgoing itinerant and evanescent states determined from the bulk lead complex band structure;^{25,35} typical energy grid spacing used in this work are 10 meV. This results in a linear system of equations at each energy E , which are solved to yield transmission matrix t with elements $t_{nm}(E)$ for each incoming channel n and outgoing channel m . The steady state charge density $\rho(r)$ can be obtained by integrating contributions from scattering states between the lead chemical potentials, assuming a Fermi–Dirac distribution occupancy specified by the incident lead chemical potential and contributions from stationary eigenstates below the lower lead chemical potential. The resulting $\rho(r)$ is then used to generate a new Hamiltonian and corresponding density following the method outlined above; this process is repeated until self-consistency in $\rho(r)$ is reached. Upon reaching self-consistency, the current is calculated using a Landauer-like formula by integrating the transmission spectrum (the square of the transmission coefficients) between the two chemical potentials.^{25,36} To map out an I – V characteristic, the entire procedure is repeated for different bias voltages.

To test the hypothesis that the NDR originates from a carbon atomic wire, connecting single-walled carbon nanotubes of diameters less than 1.0 nm,²⁶ we use a model geometry consisting of a carbon chain containing n atoms where n is between three to six, bridging (5,5) capped carbon nanotubes, as shown in Figure 1a. The cap, initially derived from half of a C_{60} molecule, is arranged so that a pentagon sits at the tip extremity, and the C_n chain symmetrically bridges equivalent atoms on the tip pentagons. The entire system is placed inside a supercell large enough so that each junction is laterally isolated from its periodic images.

The central resistive region consists of the C_n chain, nanotube caps, and four nanotube lead layers on either side of the junction, as illustrated in Figure 1a; the left and right lead regions contain four nanotube lead layers each, for a total of $220 + n$ atoms in our supercell. Relaxed structural parameters are obtained from standard DFT calculations utilizing a $1 \times 1 \times 8$ k-point sampling mesh and periodic boundary conditions along the transport or z axis; Hellmann–Feynman forces on the atoms are less than 0.1 eV/Å and each stress component is less than 1 GPa. The lead region atomic positions are fixed to bulk values obtained from separate DFT calculations.

After structural relaxation, the C_n chain is found to be bonded to a cap atom via an sp^3 bond, consistent with its 4-fold coordination. As a consequence, the carbon chain acquires a slightly bent geometry. The structure of a particular C_n chain depends on length and on whether n is even or odd. For odd chains, bond lengths are fairly constant at 1.32 Å for C_3 and range between 1.30 Å to 1.35 Å for C_5 ; for even chains, bonds alternate between 1.25 Å and 1.40 Å for C_4 , and 1.27 Å and 1.39 Å for C_6 (Figure 1b). A comparison to empirical bond lengths for single, double, and triple bonds between carbon atoms (1.54 Å, 1.34 Å, and 1.20 Å respectively) indicates double bonds between carbon atoms

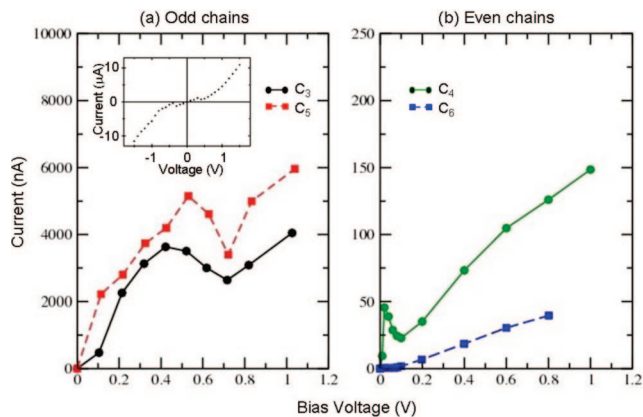


Figure 2. I – V characteristics of carbon nanotubes bridged by (a) odd carbon chains and (b) even carbon chains. Inset (from ref 26) shows experimental I – V characteristic of carbon nanotube junction exhibiting NDR.

in odd chains, while even chains exhibit behavior intermediate between the limiting case of alternating single and triple bonds (very little bond alternation is displayed by odd chains).

Further calculations within the local spin density approximation (LSDA) indicate that the system geometry remains virtually unchanged by the inclusion of spin-polarization. However, a net magnetic moment of $0.8 \mu_B$ is found for the C_3 junction, residing mainly on the carbon chain. This spin moment originates from dangling bonds localized at the cap-chain interface.³⁷ The C_4 junction also exhibits a magnetic moment of $0.9 \mu_B$, but with spin density concentrated more on the cap atoms than on the carbon chain. In this case, the magnetization is also associated with dangling bonds and unpaired spins localized in the cap region.

I – V characteristics are calculated for junctions containing carbon chains with lengths ranging from three to six atoms and appear in Figure 2. We find the shape of the I – V characteristics and bias voltages corresponding to current maxima and minima are unchanged if spin polarization effects are included, allowing us to simplify our analysis to the non-spin-polarized case.

Typical currents of junctions with even or odd carbon chains differ by about a factor of more than 50 for a given voltage range, suggesting qualitative differences in the nature of electron conduction between the two cases. Three of the four I – V curves in Figure 2 exhibit NDR, with dips in the current occurring between 0.4 to 0.7 V bias for the odd chains and below 0.1 V bias for the even C_4 chain. Interestingly, the measured I – V characteristics (inset of Figure 2a) show semiquantitative agreement with those calculated for the odd chains (Figure 2a). Our results are thus consistent with the hypothesis that the observed NDR in the nanotube junction is due to a carbon atomic wire bridging the carbon nanotubes. Further experiments would be required to establish this more definitively.

We now investigate the physical origin of the NDR and even–odd trend in the current magnitudes of these junctions. The transmission spectrum $T(E) = \text{Tr}(t^\dagger t)$, where t is the

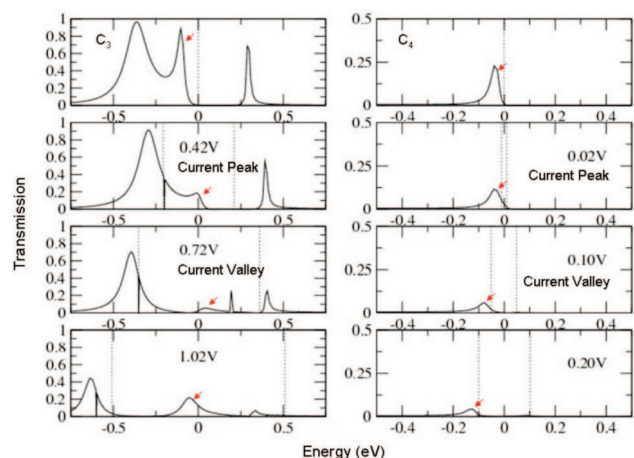


Figure 3. Transmission spectra of C_3 (left panel) and C_4 (right panel) junctions at various bias voltages. Dotted lines represent chemical potentials of the nanotube leads, and red arrows point to transmission peaks with the largest contribution to the current.

transmission matrix, is shown in Figure 3 for the C_3 and C_4 junctions at various bias voltages.

For C_3 junctions, three peaks are visible in the zero-bias transmission spectrum within a 1.5 eV energy window centered about the Fermi energy. Under a small bias, part of the transmission peak just below the lower chemical potential moves into the bias window, resulting in an initial increase in current. However, the applied bias also simultaneously reduces the peak heights, decreasing the weight of the transmission spectrum in the bias window. The overall reduction in peak height outweighs increases from additional peaks moving into the expanding bias window, leading to a net drop in current and the onset of NDR near 0.4V. For C_4 junctions, a similar explanation holds. A single peak sits just below the Fermi level in the zero-bias transmission spectrum. Under low bias, this peak begins to move into the bias window, giving rise to an initial increase in current. However, as in the C_3 junction case, the transmission peak height also decreases steadily with increasing bias, and this decrease dominates positive contributions to the current at 0.02V bias, leading to the onset of NDR.

An eigenchannel analysis shows that only one channel has a significant contribution to the transmission spectrum over the range of energies considered here. There are two incoming channels originating from the (5,5) nanotube π and π^* bands close to the Fermi level. It was found that the C_n chain reflects most of the nanotube π^* channel, and the π channel dominates conduction. The rapidly varying phase of the π^* band about the nanotube circumference gives rise to zero or near-zero coupling to the s- and p-like molecular orbitals of C_n .

To identify the nature of states giving rise to the transmission peaks, we analyze the projected density of states (PDOS) $D_i(E)$ of the scattering-state wave function on the i th pseudoatomic basis orbital $|\varphi_i\rangle$, given by

$$D_i(E) = \sum_{nk} \text{Re}(c_i^*(E_{nk}) \langle \varphi_i | \psi(E_{nk}) \rangle) \delta(E - E_{nk})$$

where $|\psi(E)\rangle$ is the scattering-state wave function, $c_i(E)$ are orbital coefficients of $|\psi(E)\rangle$ in the $|\varphi_i\rangle$ basis or

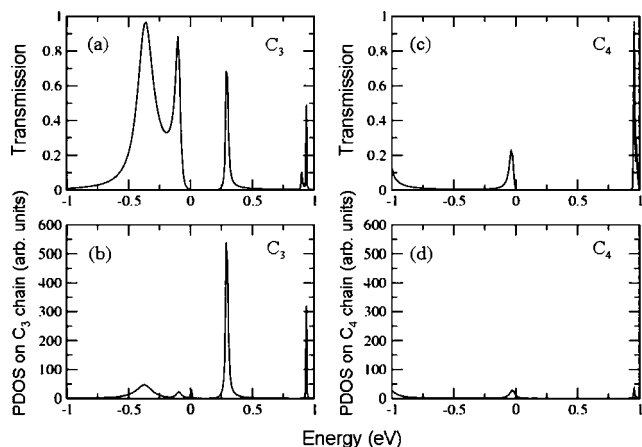


Figure 4. Zero-bias transmission (plots a and c) and projected density of states of the π -band scattering-state projected onto C_n chains for (b) C_3 and (d) C_4 junctions. The Fermi level is set to zero on the energy scale.

$|\psi(E)\rangle = \sum_i c_i(E)|\varphi_i\rangle$ and E_{nk} are energies of incident bulk-lead states. The PDOS on an atom or a group of atoms can be obtained by summing their individual orbital PDOS contributions for each atom. By using this method, the C_n chain PDOS of the zero-bias scattering-states originating from the π band is calculated and shown in Figure 4.

In the C_3 junction, analysis shows that significant PDOS with p_x character is observed near the Fermi level on the carbon chain. This PDOS originates from an eigenstate of the isolated C_3 chain (derived from atomic carbon p_x orbitals) pinned to the Fermi level by electron transfer from the leads and split into several resonances by interaction with nanotube contacts. In contrast, for the C_4 junction, there is very little PDOS near the Fermi level on the carbon chain. The most prominent feature in the PDOS is a resonance with p_x character 1.0 eV below E_F . For both C_3 and C_4 junctions, the contribution from the π -band scattering-state wave function to the PDOS projected on the nanotube lead layers of the resistive buffer and lead regions is essentially flat and featureless, reflecting the density of states of the linear π band. Evidently, the detailed transport behavior of this junction results from features in the PDOS derived from the nanotube cap and carbon chain regions.

A tight-binding model provides a simple physical interpretation for our results. (Details of the model are presented in Supporting Information.) For the C_3 junction, the model Hamiltonian parameters are adjusted to produce two states spatially localized on either side of the 3-atom carbon chain (“cap states”), with energies slightly below the lead chemical potential, and an unoccupied C_3 “chain state” that lines up with the lead chemical potential in the absence cap-chain interactions. The results of this model are illustrated in Figure 5a. From the PDOS plots, the C_3 chain and cap states hybridize into three resonances near E_F , with the low and high energy resonances localized throughout the junction region and the middle resonance localized in the cap region. Each resonance gives rise to a transmission peak, and their energetic alignment is such that a “gap-like” region opens in the transmission spectrum around the Fermi energy

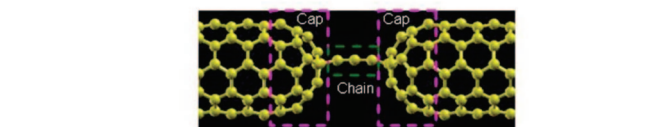
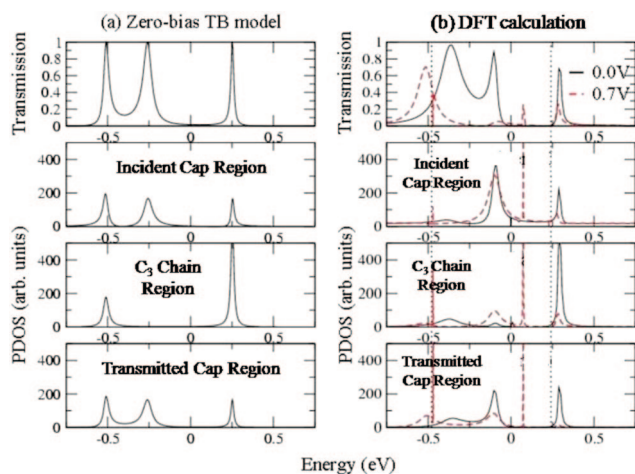


Figure 5. Transmission spectra and π -band scattering-state wave function PDOS in nanotube cap and carbon chain regions for tight-binding model (left panels) and fully atomistic scattering-state calculations (right panels) obtained for the C_3 junction. On the left panels, curves represent 0.0 V bias results. On the right panels, the solid black and dashed red curves represent 0.0 and 0.7 V bias results respectively, with the bias window defined by dotted black lines.

between the middle and the high energy peaks. (See top panel of Figure 5a) These tight-binding calculation results can be compared with those from the fully self-consistent atomistic scattering-state calculation plotted in Figure 5b, and they are qualitatively similar. This agreement validates our model and indicates that conduction is mediated by junction resonances resulting from hybridization between a carbon chain state and the nanotube cap states.

Upon application of a bias, these resonances shift and distort, as shown in Figure 5b. The change of resonance profile then leads to an increased asymmetry in the coupling, resulting in a drop of transmission peak heights and NDR in the I – V characteristics.

For the C_4 junction, we modify the tight-binding Hamiltonian to yield two localized “cap states” on either side of the carbon chain with energies slightly below the Fermi level, and a carbon “chain state” positioned far below the Fermi level (not shown in Figure 6a). Solutions of this Hamiltonian are plotted in Figure 6a. A prominent peak in the incident cap PDOS lines up well with the transmission peak energy, and the projected state density is seen to decrease dramatically as the scattering state propagates into the C_4 chain and beyond. (Note the scales for the PDOS change in the 3 left bottom panels.) Evidently in the case of C_4 , a cap state is responsible for the peak in the transmission spectrum. Moreover, since the on-chain C_4 resonance resides far below E_F , it is easier for electrons to tunnel across the junction at lower energies, producing an asymmetry in the transmission peak toward low energies in both the model and the full calculation in Figure 6. As with the C_3 case, the first-

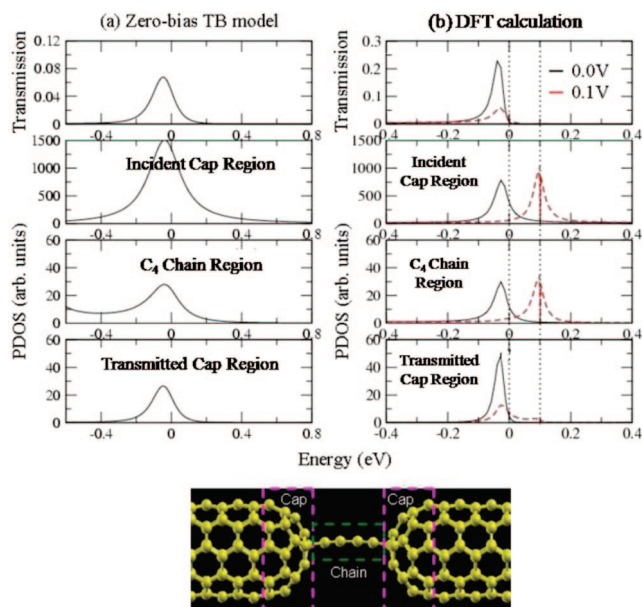


Figure 6. Transmission spectra and π -band scattering-state wave function PDOS in nanotube cap and carbon chain regions for tight-binding model (left panels) and fully atomistic scattering-state calculations (right panels) obtained for the C_4 junction. On the left panels, curves represent 0.0 V bias results. On the right panels, the solid black and dashed red curves represent 0.0 and 0.1 V bias results, respectively, with the bias window defined by dotted black lines.

principles scattering-state results, plotted in Figure 6b, agree qualitatively with the tight-binding model, validating our picture of conduction by tunneling between cap states.

With increasing voltage bias, the incident cap state shifts out of registry with the transmitted cap state. Owing to the asymmetry in the PDOS, the PDOS peak localized on the incident cap is energetically aligned to regions of low but non-negligible PDOS in the transmitted cap region, giving rise to a reduced but nonzero transmission peak. The PDOS peak localized on the transmitted cap, however, is energetically aligned to a region of near-zero PDOS on the incident cap, and this completely blocks off any transmission amplitude. The combination of these effects leads to a single transmission peak whose height decreases with increasing bias, giving rise to NDR in the I - V characteristics.

In summary, motivated by recent experiments, we performed first-principles scattering-state calculations to investigate the transport behavior of carbon nanotube junctions covalently bridged by carbon atomic chains. Semiquantitative agreement was found between the calculated and the experimental I - V characteristics, supporting the hypothesis that current may be mediated by carbon chains in the experimental nanotube junctions synthesized in ref 26. It was also found that odd numbered chains carry currents orders of magnitude larger than that in even numbered chains, owing to a qualitative difference in conduction mechanism between the two cases. Specifically, the current in odd chains are carried by resonances originating from the hybridization of nanotube cap and on-chain states, while that of even chains are mediated by electrons tunneling between nanotube cap

states. Also, it was found that both even and odd chains exhibit NDR, with that in even chains caused by an energy misalignment between cap states and that in odd chains resulting from asymmetric distortions of the conducting resonances under an applied bias.

Acknowledgment. This work was supported by National Science Foundation Grant DMR07-05941. Portions of this work were also performed at the Molecular Foundry, Lawrence Berkeley National Laboratory, and were supported by the Office of Science, Office of Basic Energy Sciences of the U.S. Department of Energy under Contract No. DE-AC02-05CH11231. Y.W.S. acknowledges support from the KRF (No. KRF-2007-314-C00093). Computational resources have been provided by the National Energy Research Scientific Computing Center and the San Diego Supercomputing Center.

Supporting Information Available: Details of a model tight-binding calculation of a carbon wire bridging carbon nanotube leads. This material is available free of charge via the Internet at <http://pubs.acs.org>.

References

- (1) Ohnishi, H.; Kondo, Y.; Takayanagi, K. *Nature* **1998**, *395* (6704), 780–783.
- (2) Ludoph, B.; Devoret, M. H.; Esteve, D.; Urbina, C.; van Ruitenbeek, J. M. *Phys. Rev. Lett.* **1999**, *82* (7), 1530–1533.
- (3) Smit, R. H. M.; Untiedt, C.; Rubio-Bollinger, G.; Segers, R. C.; van Ruitenbeek, J. M. *Phys. Rev. Lett.* **2003**, *91* (7), 076805.
- (4) CostaKramer, J. L. *Phys. Rev. B* **1997**, *55* (8), R4875–R4878.
- (5) Hansen, K.; Laegsgaard, E.; Stensgaard, I.; Besenbacher, F. *Phys. Rev. B* **1997**, *56* (4), 2208–2220.
- (6) CostaKramer, J. L.; Garcia, N.; GarciaMochales, P.; Serena, P. A.; Marques, M. I.; Correia, A. *Phys. Rev. B* **1997**, *55* (8), 5416–5424.
- (7) Thijssen, W. H. A.; Marjenburgh, D.; Bremmer, R. H.; van Ruitenbeek, J. M. *Phys. Rev. Lett.* **2006**, *96* (2), 026806.
- (8) Krans, J. M.; Vanruitenbeek, J. M.; Fisun, V. V.; Yanson, I. K.; Dejongh, L. J. *Nature* **1995**, *375* (6534), 767–769.
- (9) Rodrigues, V.; Bettini, J.; Silva, P. C.; Ugarte, D. *Phys. Rev. Lett.* **2003**, *91* (9), 096801.
- (10) Lang, N. D.; Avouris, P. *Phys. Rev. Lett.* **1998**, *81* (16), 3515–3518.
- (11) Lang, N. D.; Avouris, P. *Phys. Rev. Lett.* **2000**, *84* (2), 358–361.
- (12) Larade, B.; Taylor, J.; Mehrez, H.; Guo, H. *Phys. Rev. B* **2001**, *64* (7), 075420.
- (13) Tongay, S.; Senger, R. T.; Dag, S.; Ciraci, S. *Phys. Rev. Lett.* **2004**, *93* (13), 136404.
- (14) Neaton, J. B.; Khoo, K. H.; Spataru, C. D.; Louie, S. G. *Comput. Phys. Commun.* **2005**, *169* (1–3), 1–8.
- (15) Sim, H. S.; Lee, H. W.; Chang, K. J. *Phys. Rev. Lett.* **2001**, *87* (9), 096803.
- (16) Tsukamoto, S.; Hirose, K. *Phys. Rev. B* **2002**, *66* (16), 161402.
- (17) Lee, Y. J.; Brandbyge, M.; Puska, M. J.; Taylor, J.; Stokbro, K.; Nieminen, R. M. *Phys. Rev. B* **2004**, *69* (12), 125409.
- (18) Thygesen, K. S.; Jacobsen, K. W. *Phys. Rev. Lett.* **2003**, *91* (14), 146801.
- (19) Taylor, J.; Guo, H.; Wang, J. *Phys. Rev. B* **2001**, *63* (24), 245407.
- (20) Brandbyge, M.; Mozos, J. L.; Ordejon, P.; Taylor, J.; Stokbro, K. *Phys. Rev. B* **2002**, *65* (16), 165401.
- (21) Garcia, Y.; Palacios, J. J.; SanFabian, E.; Verges, J. A.; Perez-Jimenez, A. J.; Louis, E. *Phys. Rev. B* **2004**, *69* (4), 041402.
- (22) Xue, Y. Q.; Datta, S.; Ratner, M. A. *Chem. Phys.* **2002**, *281* (2–3), 151–170.
- (23) Di Ventra, M.; Lang, N. D. *Phys. Rev. B* **2002**, *65* (4), 045402.
- (24) Fujimoto, Y.; Hirose, K. *Phys. Rev. B* **2003**, *67* (19), 195315.
- (25) Choi, H. J.; Cohen, M. L.; Louie, S. G. *Phys. Rev. B* **2008**, *76* (15), 155420.
- (26) Yuzvinsky, T. D.; Mickelson, W.; Aloni, S.; Begtrup, G. E.; Kis, A.; Zettl, A. *Nano Lett.* **2006**, *6* (12), 2718–2722.
- (27) Yakobson, B. I.; Campbell, M. P.; Rabec, C. J.; Bernholc, J. *Comput. Mater. Sci.* **1997**, *8* (4), 341–348.

- (28) Marques, M. A. L.; Troiani, H. E.; Miki-Yoshida, M.; Jose-Yacaman, M.; Rubio, A. *Nano Lett.* **2004**, *4* (5), 811–815.
- (29) Rinzler, A. G.; Hafner, J. H.; Nikolaev, P.; Lou, L.; Kim, S. G.; Tomanek, D.; Nordlander, P.; Colbert, D. T.; Smalley, R. E. *Science* **1995**, *269* (5230), 1550–1553.
- (30) Soler, J. M.; Artacho, E.; Gale, J. D.; Garcia, A.; Junquera, J.; Ordejon, P.; Sanchez-Portal, D. *J. Phys.: Condens. Matter.* **2002**, *14* (11), 2745–2779.
- (31) Ceperley, D. M.; Alder, B. J. *Phys. Rev. Lett.* **1980**, *45* (7), 566–569.
- (32) Troullier, N.; Martins, J. L. *Phys. Rev. B* **1991**, *43* (3), 1993–2006.
- (33) Yoon, Y. G.; Mazzoni, M. S. C.; Choi, H. J.; Ihm, J.; Louie, S. G. *Phys. Rev. Lett.* **2001**, *86* (4), 688–691.
- (34) Artacho, E.; Sanchez-Portal, D.; Ordejon, P.; Garcia, A.; Soler, J. M. *Phys. Status Solidi B* **1999**, *215* (1), 809–817.
- (35) Tomfohr, J. K.; Sankey, O. F. *Phys. Rev. B* **2002**, *65* (24), 245105.
- (36) Datta, S. *Electronic Transport in Mesoscopic Systems*; Cambridge University Press: New York, 1995.
- (37) Kim, Y. H.; Choi, J.; Chang, K. J.; Tomanek, D. *Phys. Rev. B* **2003**, *68* (12), 125420.

NL8017143